Desalination and Water Treatment
www.deswater.com

doi: 10.1080/19443994.2013.800341

52 (2014) 3421–3431
April

Taylor & Francis
Taylor & Francis Group

Removal of reactive yellow dye by adsorption onto activated carbon using simulated wastewater

Abbas H. Sulaymon, Waleed M. Abood*

Department of Environmental Engineering, College of Engineering, Baghdad University, Baghdad, Iraq
Email: env_eng_waleed@yahoo.com

Received 8 June 2012; Accepted 22 April 2013

ABSTRACT

Reactive yellow dye was investigated as an adsorbate to be removed onto activated carbon during batch and continuous processes. A Fourier transform infrared (FTIR) analysis was carried out before and after onto the activated carbon adsorption. Thermodynamic parameters: Gibbs free energy, enthalpy change, and entropy change were found at different temperatures. Isotherm experiments were carried out at different conditions: adsorbent dosage (0.1–0.5 g), temperature (20–50 °C), pH (2.5–9), and initial concentration (50–150 mg/l). Langmuir, Freundlich, and (Brunauer, Emmet, and Teller) BET isotherm model were used to fit the results. Kinetics mechanism of mass transfer pseudo-first-order, pseudo-second-order, and intraparticale diffusion models were studied. Fixed bed column experiments were carried out at different bed heights (0.05–0.15 m), initial concentration (10–50 mg/l), and flow rate (4–12) 10^{-6} m^3/min to find empty bed contact time at break though point. Bed depth service time model was used as a shortcut model to predicate the breakthrough curves comparing with experimental data.

Keywords: Reactive yellow dye; FTIR; Activated carbon; Adsorption

1. Introduction

Reactive dyes are widely used for textile dyeing, paper printing, leather dyeing and color photography, and as additives in petroleum products. Contamination of water resources with dyes is not desirable since it damages the aesthetic nature of water and reduces the light penetration degree into the water's surface. Furthermore, the colored effluents may contain toxic carcinogenic, mutagenic, or teratogenic chemicals for microbes and fish species. Approximately 10,000 different dyes and pigments are used in industry, most of them are difficult biodegrade because they have complex aromatic molecular structures and synthetic origins [1].

Wastewater from the process textile finishing industry commonly contains moderate concentrations (10–200 mg/l) of dyestuffs, contributing significantly to the pollution of aquatic ecosystems. The reactive dyes, which represent the largest class of dyes used in textile processing industries, are almost azo compounds, i.e. molecules with one or several azo (N=N) bridges linking substituted aromatic structures. These dyes are designed to be chemically and photolytically stable, and they exhibit a high resistance to microbial degradation and are highly persistent in natural environment. The release of these compounds into the

*Corresponding author.

environment is undesirable, not only for aesthetic reasons, but also because many azo dyes and their breakdown products are toxic and/or mutagenic for life [2].

Traditional physicochemical and biological treatment methods are ineffective to remove the reactive dyes. The widely used methods to treat wastewater containing dyes are chemical precipitation, ion-exchange, reverse osmosis, ozonation, solvent extraction, adsorption, membrane filtrations, flocculation, and advanced oxidation process [3].

Within these techniques, adsorption technology has been widely applied to treat dyes wastewater using various adsorbents such as activated carbon (AC), peat, chitin, sludge, algae, clay, zeolite, clay, fly ash, and montmorillonite. Although AC is relatively expensive compared to other materials, it has been used as a common adsorbent because of its large surface area and high adsorption capacity to organics [4].

The aim of this study is to investigate experimentally and theoretically, the removal of reactive yellow dye FG (Remazol yellow 42) by granular activated carbon in batch and fixed bed processes.

Batch process was carried out at different conditions (temperature, pH, adsorbent dosage, contact time, and initial concentration). Fixed bed process was carried out at different variables (flow rate, bed height, and initial concentration).

2. Mathmetical models

2.1. Adsorption isotherms models

Equilibrium data is commonly known as adsorption isotherms are the basic requirements for the design of the adsorption systems. These data provide information on the capacity of the adsorbent or the amount required to remove a unit mass of pollutant under the system conditions.

Langmuir, Freundlich, and (Brunauer, Emmet, and Teller) BET isotherm models are used to describe the equilibrium characteristics of adsorption. Linear regression is commonly used to determine the best-fit model [5].

Langmuir isotherm, applicable for homogenous surface adsorption, is given as:

$$q_e = \frac{q_m K_L C_e}{1 + K_L C_e} \tag{1}$$

Eq. (1) can be rearranged into linear form:

$$\frac{C_e}{q_e} = \frac{1}{q_m K_L} + \frac{C_e}{q_m} \tag{2}$$

By plotting C_e/q_e vs. $1/C_e$, the Langmuir constants can be obtained.

One of the most popular adsorption isotherm model used for the liquids to describe adsorption on a surface having heterogeneous energy distribution is Freundlich isotherm. It is given as:

$$q_e = K_F C_e^{(\frac{1}{n})} \tag{3}$$

Freundlich isotherm model is derived assuming heterogeneity surface. K_F and n are indicators of adsorption capacity and adsorption intensity, respectively. Rearranging Eq. (3) by taking logarithm:

$$\log(q_e) = \log(K_F) + \frac{1}{n}\log(C_e) \tag{4}$$

A plot of log q_e vs. log C_e yields a straight line, with a slope of 1/n and intercept of log K_F. The value of Freundlich constant (n) should lie in the range of 1–10 for favorable adsorption.

BET isotherm model is a theoretical equation and is classified under multilayer physisorption isotherm [5] is given as:

$$q_e = \frac{q_m K_b C_o C_e}{(C_o - C_e)[C_o + C_e(K_b - 1)]} \tag{5}$$

Rearranging Eq. (5) to get:

$$\frac{C_e}{q_e(C_o - C_e)} = \frac{1}{q_m K_b} + \frac{(K_b - 1)C_e}{(q_m K_b)C_o} \tag{6}$$

A plot of $[C_e/q_e\ (C_o - C_e)]$ vs. $(C_e/C_o$ yields a straight line, with a slope of $[(K_b\text{-}1)\ /K_b\ q_m]$ and intercept of $(1/K_b\ q_m)$.

2.2. Adsorption kinetic models

The transient behavior of the dye sorption process is analyzed by using the pseudo-first-order, pseudo-second-order, and intraparticle diffusion models in order to explore the potential rate controlling steps [6] involved in the adsorption of yellow dye onto AC.

2.2.1. Pseudo-first-order model

The pseudo-first-order kinetic model has been widely used to predict dye adsorption kinetics. The pseudo-first-order rate expression suggested originally by Lagergren is based on the solid capacity is expressed as follows:

$$\frac{dq_t}{dt} = K_1(q_e - q_t) \quad (7)$$

After integration and after applying the boundary conditions:$q_t = 0$ at $t = 0$ and $q_t = q_e$ at $t = t$.

The integrated form becomes Eq. (8):

$$\log(q_e - q_t) = logq_e - \frac{K_1 t}{2.303} \quad (8)$$

Values of qe and K_1 can be obtained from the slope and intercept of the plot log (qe − qt) vs. t.

2.2.2. Pseudo-second-order model

Pseudo-second-order model is shown by the following equation:

$$\frac{dq_t}{dt} = K_2(q_e - q_t)^2 \quad (9)$$

For the boundary conditions:
$q_t = 0$ at $t = 0$ and $q_t = q_e$ at $t = t_e$

$$\frac{t}{q_t} = \frac{1}{K_2 q_e}^2 + \frac{t}{q_e} \quad (10)$$

Values of q_e and K_2 can be obtained from the slope and intercept of the plot t/q_t vs. t, respectively.

2.2.3. Intraparticle diffusion model

An intraparticle diffusion rate can be expressed in terms of the square root time. The mathematical dependence of q_t vs. $t^{0.5}$ is obtained if the sorption process is considered to be influenced by diffusion in the spherical particles and the convective diffusion in the solution. The root time dependence, the intraparticle diffusion model [6] is defined as follows:

$$qt = K_i t^{0.5} + I \quad (11)$$

The plot q_t vs. $t^{0.5}$ is given by multiple linear regions representingthe external mass transfer followed by intraparticle or pore diffusion [6].

2.3. Thermodynamic study

Thermodynamic parameters Gibbs free energy change (*G*), enthalpy change, and (*H*) entropy change (*S*) are obtained from the experiments carried out at different temperatures. The free energy of adsorption can be related with Langmuir adsorption constant [7] by the following equation:

$$\Delta G = -RT \ln K_d \quad (12)$$

where K_d is equilibrium isotherm constant.

Therefore, enthalpy and entropy changes can be estimated from the following equation:

$$\ln K_d = -\frac{\Delta G}{RT} = \frac{\Delta S}{R} - \frac{\Delta H}{RT} \Delta H = T\Delta S + \Delta G \quad (13)$$

Thus, a plot of ln K_d vs. 1/T is a straight line. Δ H and Δ S values are obtained from the slope and intercept of this plot, respectively.

2.4. Bed depth service time model (BDST)

Bed service height model is a simple model that assumes a linear relationship between bed height and service time of a column. This can be expressed by Eq. (14) [6, 8]:

$$t = \frac{N_o Z}{C_o U_o} - \frac{1}{K_a C_o} \ln\left(\frac{C_o}{C} - 1\right) \quad (14)$$

$$\ln\left(\frac{C_o}{C} - 1\right) = \frac{K_a N_o Z}{U_0} - K_a C_o t \quad (15)$$

This model ignores the intraparticle mass transfer resistance and external film resistance. With these assumptions, the model reasonably fits the many packed bed adsorption systems well and provides information (N_o and K_a) useful for the scale up of a given adsorption system.

3. Experimental materials and method

3.1. Adsorbent

Granular activated carbon was used as adsorbent with diameter (0.5–0.75 mm), bulk density 711.8 kg/m^3, porosity 53, 44%, and surface area 911.56 m^2/g.

AC was washed with distilled water to remove dust and fine particles then dried at 100 ˚C.

3.2. Adsorbate

A yellow FG reactive dye (Remazol yellow 42) was obtained from Iraqi textile factory as a powder with solubility 150 g/l as recorded by the manufactured companies. A stock of dye solution was prepared by dissolving the required amount of dye in distilled water. Due to commercial reasons and unavailable chemical structure of their product, the suppliers consider these specifications as know how [9,10].

The dye was measured at a maximum wave length 420 (nm) using double beam spectrophotometer (Labomed, UVD. 3,500 USA) and single beam spectrophotometer type (APEL PD- 303 UV JAPAN) which was used for the analyzing of samples [11,12].

3.3. Fourier transform infrared (FTIR)

Fourier transform infrared (FTIR) technique was used to examine the surface groups of the adsorbent and to identify those groups responsible for dye adsorption. Adsorption in the IR region takes place because of the rotational and vibrational movements of the molecular groups and the chemical band of the molecule [13].

FTIR technique was used to identify the characteristics of the functional group for the adsorbent surface of AC (before and after adsorption). FTIR analyses were carried out (FTIR type Spectrlab, MB 3,000, ABB, U.K) by mixing the samples with potassium bromide, pressed and scanned at 4,000–400 cm^{-1} [14].

An uptake percentage was calculated using the following equation:

$$\text{Uptake}\% = \frac{C_0 - C_e}{C_0} 100 \quad (16)$$

The amount of adsorbed solute per mass of adsorbent was calculated using the following equation:

$$q_e = \frac{C_0 - C_e v}{m} \quad (17)$$

3.4. Isotherm experiments

The batch adsorption isotherm experiments were carried out by varying initial dye concentrations (50, 100, and 150 mg/l), initial pH (2.5, 4, 6.3, and 9) ±0.2, temperature (20, 35, and 50˚C) ± 2, and adsorbent dosage (0.1, 0.15, 0.2, 0.3, 0.4, and 0.5). In each experiment accurately weighed AC was added to 100 cm^3 of aqueous dye solution taken in a 300 cm3 glass bottle and the mixture was agitated at 200 rpm in a shaker at a constant temperature. Samples were drawn after 5 h and filtered by filter paper. The dye concentration was determined using UV–vis spectrophotometer.

3.5. Kinetic experiments

The batch adsorption kinetic experiments were carried out by varying initial dye concentrations (50, 100, and 150 mg/l), initial pH (2.5, 4, 6.3, and 9) ±0.2, and temperature (20, 35, and 50˚C) ± 2. In each experiment 0.5 g AC was added to 0.5 l of aqueous dye solution placed in a 1 l glass container, the mixture was agitated at 200 rpm by heating magnetic stirrer at a desired constant temperature. Samples were drawn at different time intervals and filtrate by filter paper. The dye concentration was determined using spectrophotometer.

3.6. Fixed bed column experiments

Removal of yellow dye in continuous process was investigated using packed bed of AC in perspex column with internal diameter 0.0125 m and length 0.5 m at different conditions, bed height (0.05, 0.1, and 0.15 m), dye concentration (10, 25, and 50 mg/l), and flow rate (4, 7.5, and 12) 10^{-6} m^3/min.

At the top of the packing bed, a layer of glass bead was used to provide uniform inlet flow to the column and the same layer was placed at the bottom to prevent discharging any AC particles during sampling.

Dye solution was introduced into the column at different flow rates by gravity, and was controlled by the level flow from an elevated feeding tank. The flow rate was measured by the means of a rotameter and adjusted with needle valve. Samples were collected at regular time intervals.

Empty bed contact time (EBCT) was calculated to find the resident time of the solution in the column Eq. (18) [9].

$$\text{EBCT} = \frac{V_b}{Q} = \frac{Z}{U_0} \quad (18)$$

4. Result and discussion

4.1. FTIR analyses

Fig. 1 shows the FTIR before and after adsorption at pH (6.3). It can be seen that there is clear change in bands (3,416–3550 cm^{-1}) which assigned to the [O–H] stretching [15] that increases due to [O-H] form dye which is anionic type. The other functional group at peaks (1,210–1,738 cm^{-1}) refers to C=O before adsorption which had been masking by the yellow dye.

The peak (1,617 cm^{-1}) shows increasing in intensity of aromatic C=C ring stretching [16] may be caused by dyes structure that can be seen as small peak by near to C=C of –N=N– stretching [13].

4.2. Equilibrium adsorption study

4.2.1. Effect of adsorbent dosage

Adsorbent dosage can increase the percentage of dye removal from the solution. This is expected because by increasing the adsorbent dosage, the

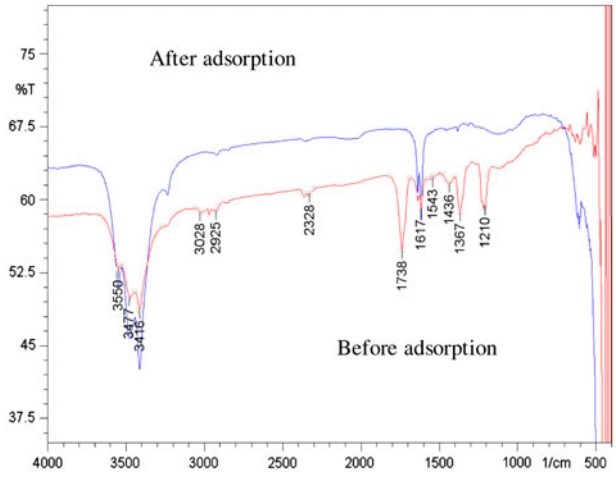

Fig. 1. FTIR for AC before and after adsorption of yellow dye.

number of adsorption sites available for adsorbent–adsorbate interaction is increased Figs. 2, 3, and 5 [1].

4.2.2. Effect of temperature

Fig. 2 shows an increase of uptake per cent with increasing temperature along with increase in mass of adsorbent. This is probably due to the fact that at higher temperatures an increase in free volume occured and it leads to an increment in the mobility of the solute [16].

4.2.3. Effect of pH

Fig. 3 shows an increase in the adsorption capacity with the decrease in the pH from 2.5 to 6.3 and then it increases with the increasing pH from 6.3 to 9 for all the adsorbent mass. Constant adsorption capacity of activated carbon for dyes was observed at pH

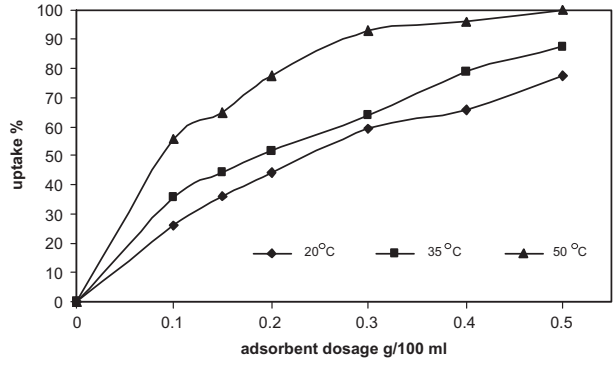

Fig. 2. Effect of temperature on yellow dye uptake percentage.

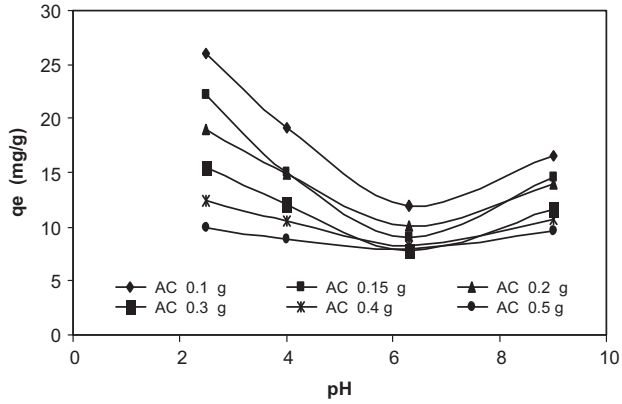

Fig. 3. Effect of adsorbent dosage on adsorption capacity at different pH.

range 4–8 for 0.4–0.5 g adsorbent was an indication that the availability of adsorption sites and electrostatic mechanism were not the only mechanism for dye adsorption in this system [5]. They showed that the removal capacity increases at pH >7 due to the neutral protonated groups of activated carbon which are mainly carboxylic group (–CO–OH^+) and phenolic (–OH^+), while there are positive groups (SO_3H^+) or partially positive charges of dye[17–19] which interact with (OH^-) of solution.

4.2.4. Effect of initial concentration

Fig. 4 shows that the adsorption capacity increases with the increase in initial concentration at all adsorbent mass due to the initial concentration which acts as a driving force to overcome the resistances of the mass transfer of the dye between the solution bulk and the adsorbent surface [18].

4.3. Adsorption isotherm models

Different adsorption isotherm model were used to fit the experimental data. The constant variables of these models were found using Eqs. (2, 4, and 6) and listed in Table 1. While examining Table 1 it can be seen that the results show good fitting with BET model then the other models with high R^2 values at different temperatures pH and initial concentration (0.92–0.99), (0.91–0.99), and (0.9–0.97), respectively, which refers to multilayer formation of adsorbate on the surface of adsorbent [5].

Maximum obtained adsorption capacity (q_m) increases in all models with increase in temperature and initial concentration. This due to opening new of

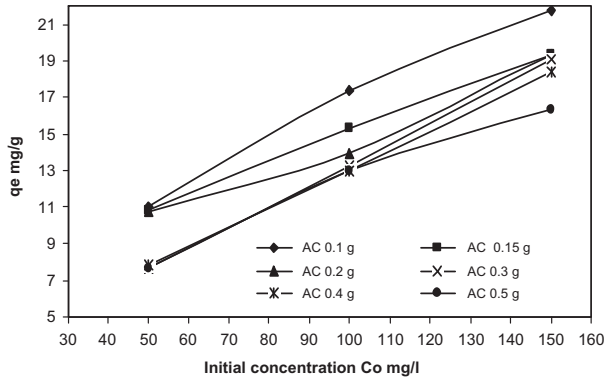

Fig. 4. Effect of adsorbent dosage on adsorption capacity at different initial concentration.

closed pores and more transferred molecules into them.

K_L values was increased at q_m increases at different temperature and pH but decreases by increasing initial concentration and this relation is affected by intercept of linear line of Eq. (2).

For pH at acidity and alklinity shows increasing in adsorption capacity for all the models with increasing the R^2 values.

4.4. Thermodynamic studies

ΔG, ΔH, and ΔS values were obtained from Eq. (13) and are given in Table 2. Values of ΔG for adsorption onto AC were negative (−24.34,−41.82, and −59.3 kJ/mol at 293, 303, and 323 K, respectively), which were rather low, indicating that spontaneous adsorption had occured. ΔH and ΔS of adsorption were + 317.2 kJ/mol and 1.165 kJ/mol K, respectively.

Table 2
Thermodynamic properties

Temp. ℃ (K)	ΔG (kJ/mol)	ΔH (kJ/mol)	ΔS (kJ/mol K)
20(293)	−24.34	+317.2	+1.165
35(308)	−41.82		
50(323)	−59.3		

The positive value for Δ H confirms that the overall adsorption of yellow dye onto AC is an endothermic process. The positive value ΔS reflects the affinity of the AC for yellow dye and increased randomness at the solid/solution interface with some structural changes of the adsorbent [6, 16] as shown by FTIR after adsorption.

4.5. Kinetic adsorption study

4.5.1. Effect of temperature

Fig. 5 shows the effect of contact time on adsorption at different temperatures, and equilibrium was almost established within 2 h. A high increase rate of q_m at the beginning for all temperatures followed by slow mass transfer until it became near to steady state after 4 h; this is due to the high temperature where the molecules have more ability to be free to move towards the pores [2]. The adsorption capacity increased with temperature and it is probably due to the increase of intraparticle diffusion rate of the adsorbate into the interior sites of the adsorbent, since diffusion is an endothermic reaction [16].

Table 1
Langmuir, Freundlich, and BET constants for the adsorption of yellow dye at different conditions

Conditions	Langmuir model			Freundlich model			BET model	
	q_m	K_L	R^2	K_F	n	R^2	q_m	R^2
Temperature, 20 ℃ (293 K)	16.7	0.075	0.82	2.92	2.5	0.65	3.26	0.92
35 ℃ (308 K)	21.9	0.076	0.86	4.1	2.61	0.86	5.95	0.98
50 ℃ (323 K)	27.1	0.448	0.95	9.9	3.3	0.987	15.36	0.99
pH								
2.5	25	0.69	0.97	12.95	5.26	0.93	13.9	0.99
4	22.4	0.11	0.93	4.7	2.61	0.93	7.15	0.99
6.3	12.4	0.115	0.81	4.45	4.4	0.44	2.64	0.91
9	17.3	0.244	0.96	8	5.6	0.86	5.88	0.96
Initial concentration, mg/l								
50	12.3	0.108	0.82	3.9	4	0.465	2.4	0.9
100	19.5	0.044	0.73	6.37	5.1	0.32	3.02	0.97
150	27.6	0.023	0.94	4.44	3.15	0.78	3.15	0.92

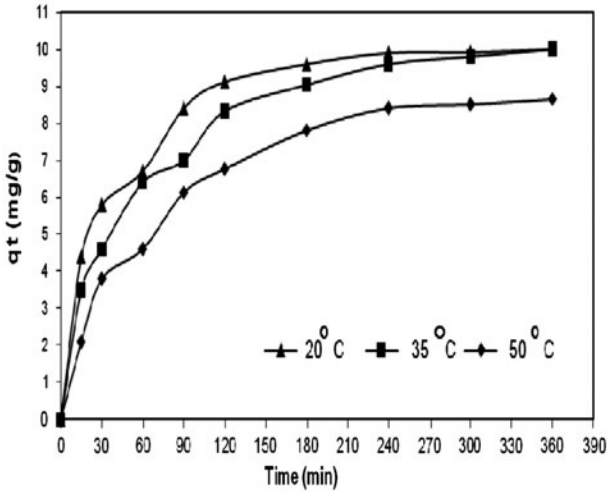

Fig. 5. Adsorption capacity at different temperature.

4.5.2. Effect of pH

Fig. 6 shows the increase in the adsorption capacity at acidity and alkalinity condition with an increase in the contact time in batch process to reach a 100% uptake at pH 2.5 and 9. This is due to the amphoteric behavior of AC (acid–base behavior). This results in agreement with other researchers [20] who showed that this behavior make the activated carbon to manifest reactivity for many organic and inorganic adsorbates.

4.5.3. Effect of initial concentration

Adsorption capacity Fig. 7 increases with increasing initial concentration with increasing contact time due to the difference in concentration which plays a role as driving force that leads the molecules of the adsorbate to occupy all available adsorbate sites

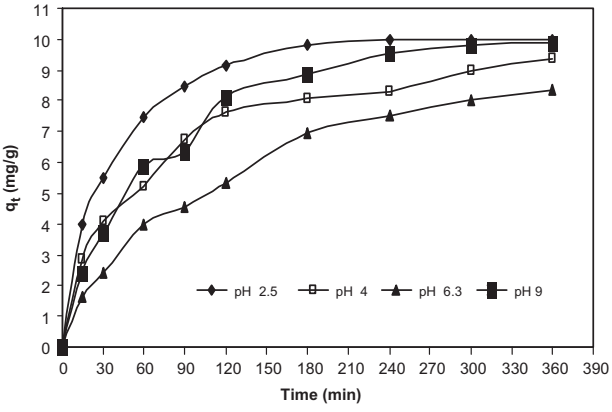

Fig. 6. Adsorption capacity at different pH.

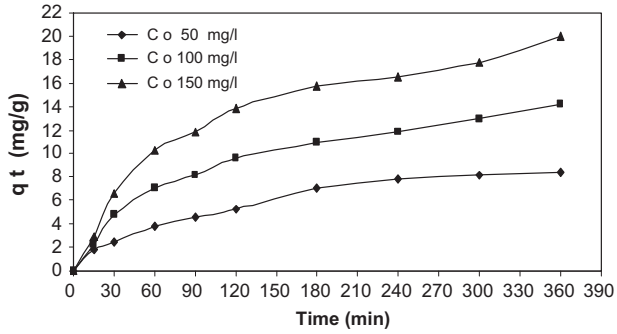

Fig. 7. Adsorption capacity at different initial concentration.

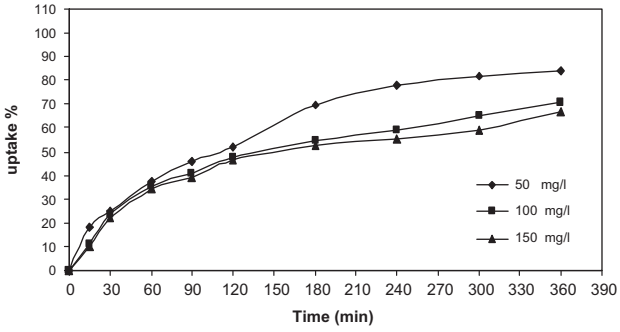

Fig. 8. Dye uptake percentage at different initial concentration.

which shows the fitting with Langmuir and BET models at C_o equal 150 mg/l. Fig. 8 shows the same response even at the first stage of uptake but the uptake percentage of yellow dye decreased (84%, 71%, and 66.7%) with increasing initial concentration (50, 100, and 150 mg/l), respectively, at constant adsorbent mass (0.5 g). This phenomenon is due to rapid attachment of dye molecules to the surface of AC which leads to fast removal at low concentration [16].

In order to explore the potential rate controlling steps [15] involved in the adsorption of yellow dye by AC kinetic models Eqs. (8, 10 and 11) were used to express and compare the experimental adsorption capacity (q_{exp}), and the calculated by pseudo-first-order, pseudo-second–order, and intraparticle diffusion model to examine the stability of the adsorption process [21] Table 3.

From the results fittings by both pseudo-first-order and pseudo-second-order models with R^2 rank (0.98–0.99) and (0.988–0.999), respectively, show that the limiting step cannot be determine by one of these models [6]. The most calculated q_{cal} adsorption capacity was near the actual ones in each condition.

R^2 values of intraparticle diffusion model were less than other models due to that there are two mechanisms to be considered which are Fig 9.

Table 3
Kinetic parameters at different conditions

Conditions	q_{exp}	Pseudo-first-order			Pseudo-second-order			Intraparticle diffusion	
		q_{cal}	$K_1\ 10^{-3}$	R^2	q_{cal}	$K_2\ 10^{-3}$	R^2	K_i	R^2
Temperature									
20 °C (293 K)	8.64	8.52	13.8	0.99	10.12	16.7	0.997	0.428	0.926
35 °C (308 K)	10	7.91	12.2	0.99	11.17	2.1	0.998	0.433	0.928
50 °C (323 K)	10	6.93	16	0.98	10.8	3.6	0.999	0.365	0.86
pH									
2.5	10	8.54	20.2	0.99	10.8	3.7	0.999	0.378	0.83
4	9.35	6.78	9.2	0.96	10.4	2	0.996	0.414	0.93
6.3	8.35	8.78	10.3	0.98	10.7	0.88	0.99	0.465	0.98
9	9.9	10.6	14.7	0.93	11.7	1.36	0.997	0.503	0.92
Initial concentration, mg/l									
50	8.4	9.52	11.5	0.98	10.84	0.885	0.983	0.468	0.98
100	14	12.1	7.4	0.99	17.27	0.6	0.99	0.734	0.97
150	20	15.85	6.7	0.98	24.1	0.45	0.988	1.023	0.95

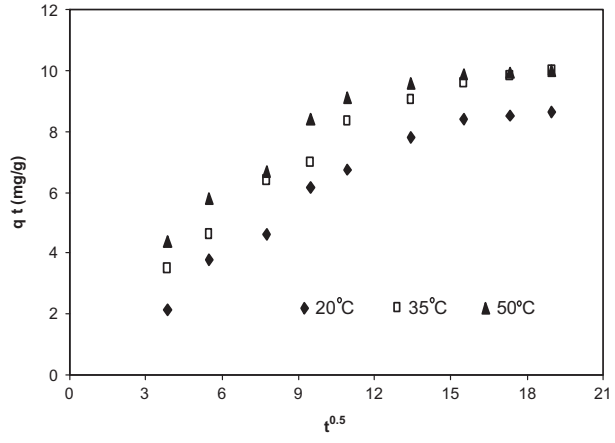

Fig. 9. Intraparticle diffusion model for yellow removal by 0.5 g AC at different temperature.

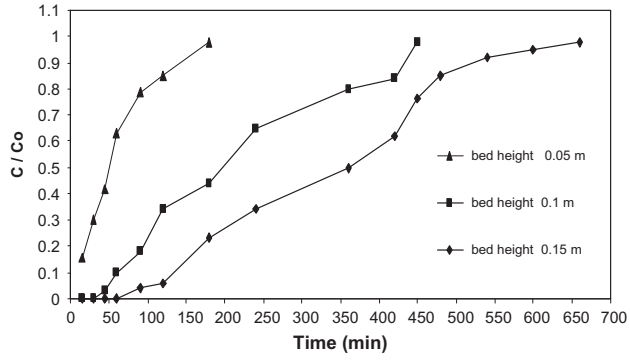

Fig. 10. Breakthrough curve of yellow dye removal at different bed height, initial concentration = 50 mg/l, and flow rate = $12 \times 10^{-6} m^3/min$.

First is the initial linear portion which is attributed to the bulk diffusion, and the second is to intraparticle / pore diffusion [6, 22] shows that the intraparticle diffusion is not the only rate-limiting mechanism [16].

4.6. Column experiments

4.6.1. Effect of bed height

Breakthrough curves are shown in Fig. 10 for the different bed heights (0.05, 0.1, and 0.15 m) at and ($12 \times 10^{-6} m^3/min$). This Figure shows that the break through time increase with increasing the bed height (0, 80, and135 min), respectively, the increase in the bed height will increase the volume of bed, and then the increases at calculated EBCT using Eq. (18) are (0.51, 1.02, and 1.53 min) [8].

4.6.2. Effect of initial concentration

Decreasing an initial concentration (50, 25, and 10 mg/l) leads to the increase in the service bed time with breakthrough time (0, 60, and 180 min), respectively Fig. 11. This is due to the driving force that acts at high concentration [23] which saturates the nearest available sites. Without enough contact time between adsorbent and adsorbate will prevent the adsorption process to be completed and to reach the breakthrough time.

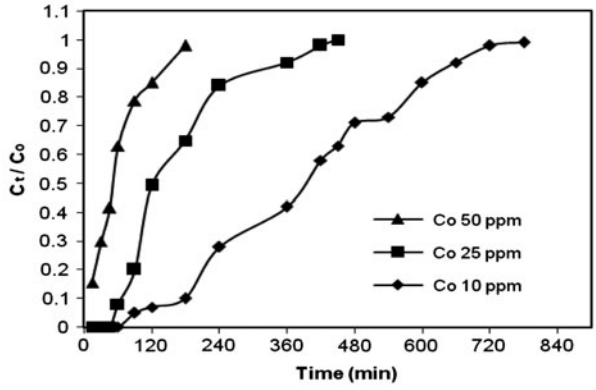

Fig. 11. Breakthrough curve of yellow dye removal at different initial concentration, bed height = 0.05 m, and flow rate = 12×10^{-6} m3/min.

4.6.3. Effect of flow rate

The effect of the flow rate on the adsorption of yellow dye is shown in Fig. 12. This Figure shows that a decrease in flow rate (12, 7.5, and 4) 10^{-6} m^3/min (at constant AC bed height and initial concentration of dye) leads to an increase EBCT (0.51, 0.817, and 1.533 min) and breakthrough time (0, 30, and 65 min), respectively.

It was observed that breakthrough generally occurred faster with higher flow rate due to higher rate of mass transfer, thus the amount of yellow dye adsorbed onto AC bed (mass transfer zone) increased, but the adsorption capacity will be lower due to insufficient residence time of the solute in the column and diffusion of the solute into the pores of the adsorbent. Therefore the solute left the column before equilibrium occurred [23]. At high flow rate the thickness of the film around the adsorbent will be reduced, as well as the resistance to adsorbate transfer.

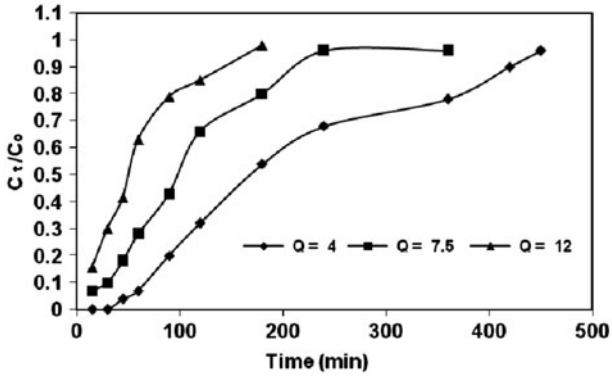

Fig. 12. Break through curve of yellow dye removal at flow rate [Q* (10^{-6})]m^3/min, initial concentration = 50 mg/l and bed height = 0.05 m.

Table 4
BDST model constants

conditions	BDST model parameters		
	K_a 10^{-5}	No	R^2
Bed-depth, m			
0.05	64.5	5,547.2	0.98
0.1	23.6	10,067	0.906
0.15	23.2	10,995.8	0.979
Co mg/l			
10	10.2	7,526.3	0.976
25	61.6	8,163.4	0.935
50	65	5,546.1	0.977
Q, ml/min			
4	26.2	7,212	0.927
7.5	36	7,417.8	0.9
12	64	5,532.2	0.978

Using Eq. (15) the parameters of the model were calculated by plotting $(\ln(\frac{C_o}{C} - 1) vs. t)$, and K_a and N_o were estimated from slope and intercept of the line Table 4.

R^2 values show good fitting with BDST model at different bed height, initial concentration, and flow rate (0.906–0.98), (0.935–0.977), and (0.9–0.978), respectively. The slope and intercept of the model were found to be effected by process conditions.

K_a values were calculated from the slope of the line of BDST model which shows that they increase with decreasing bed heights, and increases with increasing initial concentrations and flow rates. This is due to the rate parameter K_a depending on the effect of both external film diffusion mass transport, which varies with fluid velocity, and interparticle diffusion, which is independent of fluid velocity [24].

EBCT decreases with increasing the flow rate. High K_a values remain to increase may be due to high velocity and film diffusion which became more active when leading to increase the mass transfer rate. The variation in concentration shows no changes in EBCT or velocity but the change in K_a values were due to an effect of mass transfer (different in concentration which act as driving force role).

The values of N_o were calculated using the intercept of the linear form of BDST model, N_o increases with increasing bed height, initial concentration (>25 mg/l), and flow rate (>7.5×10^{-6} m^3/min) [24] due to high bed height, and low flow rate will increase the bed surface area and the contact time of adsorbate–adsorbent and more efficient removal. Low concentrations reduce the rapid saturation of bed, and increase the bed service time.

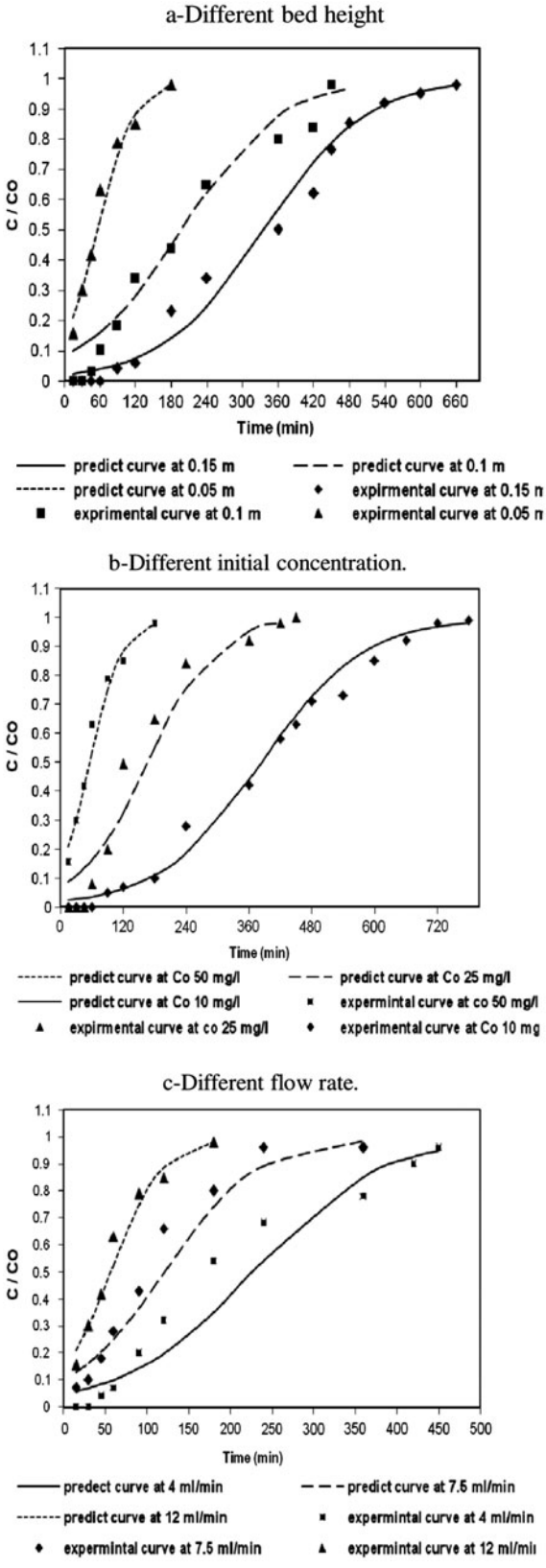

Fig. 13. (a, b, and c) Experimental and predict break through curves.

Fig. 13(a–c) shows a good fitting between experimental and predicted break through curves values using BDST model for different bed height, initial concentration, and flow rates.

5. Conclusions

- FTIR shows physical–chemical adsorption of yellow dye onto activated carbon.
- AC behaves as acid–base to adsorb yellow dye at high and low pH.
- Effect of temperature and pH show an increase of adsorption capacity and uptake percentage of AC at different adsorbent dosages and contact time.
- Increasing initial concentration shows the increase of adsorption capacity q_t with decreasing adsorbent dosage, while uptake percentage increases at decreasing of initial concentration.
- Isotherm models show the best fitting with BET model mean adsorption of multilayers.
- Kinetic results show well fitting with pseudo-first and second-order model and intraparticle diffusion model involve bulk diffusion.
- Fixed—bed column results show increase in breakthrough time at increasing bed height, and decreasing initial concentration and flow rate.
- BDST model shows good fitting with experimental data to predict the breakthrough curve at different bed heights, initial concentrations, and flow rates with R2 values (0.906–0.98), (0.935–0.977), and (0.9–0.978), respectively.

Nomenclature

C — dye concentration in aqueous solution (mg/l)
C_e — equilibrium dye concentration in liquid phase (mg/l)
C_o — initial dye concentration in aqueous solution (mg/l)
ΔG — free energy of adsorption (kJ mol^{-1})
ΔH — entropy change (kJ mol^{-1})
K_a — BDST model constant (l/mg min)
K_b — BET model constant
K_i — intraparticle diffusion rate constant (mg g^{-1} min$^{0.5}$)
K_F — Freundlich constant (mg g^{-1})
K_L — Langmuir adsorption constant (l mg^{-1})
K_1 — pseudo-first-order rate constant (min^{-1})
K_2 — pseudo-second-order rate constant (g mg^{-1} min^{-1})

m — adsorbent dosage (g)
n — Freundlich parameter
N_o — the sorption capacity of the bed per unit volume of the bed (mg/l)
Q — flow rate (m^3/min)
q_t — amount of dye adsorbed per unit mass of adsorbent at time t ($mg\,g^{-1}$)
q_m — Langmuir isotherm parameter, maximum dye adsorbed/unit mass of adsorbent ($mg\,g^{-1}$)
q_e — aquilibrium dye concentration in solid phase ($mg\,g^{-1}$)
R — gas universal constant (0.08314 kJ/mol K)
ΔS — entropy change ($kJ\,mol^{-1}\,K^{-1}$)
T — temperature C (K)
t — time (min)
t_b — column break through time (min)
U_o — superficial velocity of the solution (m/min)
$_V$ Sample volume for isotherm and kinetic experiments (m^3)
V_b — bed volume (m^3)
Z — bed height (m)

References

[1] F. Li, C. Ding, Adsorption of reactive black dye on different deacetylation degree chitosan, J. Eng. Fibers Fibrics 6 (2011) 25–31.
[2] D. Suteu, D. Bilba, Equilibrium and kinetic study of reactive red dye HE-3B adsorption by activated carbon, Acta Chimica Slovenica 52 (2005) 73–79.
[3] L. Shi, N. Li, C. Wang, Catalytic oxidation and spectroscopic analysis of simulated wastewater containing o-chlorophenol by using chlorine dioxide as oxidant. J. Hazard. Mater. 178 (2010) 1137–1140.
[4] H.D. Choi, M. Shin, D. Kim, C. Jeon, K. Baek, Removal characteristics of reactive black 5 by surfactant modified activated carbon, Desalination 223 (2008) 290–298.
[5] K.Y. Foo, B.H. Ahmed, Insight into the modeling of adsorption isotherm Systems, Chem. Eng. J. 156 (2010) 2–10.
[6] V. Ponnusami, S. Vikram, Guava (*Psidium guajava*) leaf powder: Novel adsorbent for removal of methylene blue from aqueous solution, J. Hazard. Mater. 152 (2008) 276–286.
[7] V.S. Mane, I.D. Mall, V.C. Srivastava, Use of bagasse fly ash as an adsorbent for the removal of brilliant-green dye from aqueous solution, J. Dyes Pigm. 73 (2007) 269–278.
[8] W.J. Thomas, B. Crittenden, Adsorption Technology and Design, Butterworth Heinemann, Oxford, 1998.
[9] Y.S. Al M.-Degs, M.A. Khraisheh, S.J. Allen, M. Ahmed, Adsorption characteristics of reactive dyes in column of activated carbon, J. Hazard. Mater. 165 (2009) 944–949.
[10] M.A. Al-Gouti, M.A. Khraisheh, S.J. Allen, M. Ahmed, Adsorption of heavy metals ions onto modified diatomite, J. Hazard. Mater. 146 (2007) 316–327.
[11] O. Karmo, Adsorption the dyes from effluent of textile factories by activated carbon, Al-Assad J. Eng. Sci. Univ. Damascus 23 (2007).
[12] S.T. Ong, P.S. Keng, C.K. Lee, Basic and reactive dyes Sorption by modified rice hull, Am. J. Appl. Sci. 7 (2010) 447–452.
[13] S. Kara, C. Aydiner, E. Demirbas, N. Dizge, Modeling the effects of adsorbent dose and particle size on the adsorption of reactive textile dyes by fly ash, Desalination 212 (2007) 282–293.
[14] M. Haris, K. Sathasivam, The removal of methyl red from aqueous solutions using banana pseudostem fibers, Am. J. Appl. Sci. 6 (2009) 1690–1700.
[15] R.A. Shawabkeh, Adsorption of chromium ions from aqueous solution by using activated carbo- alumino silicate material from oil shale, J. Colloid Interface Sci. 299 (2006) 530–536.
[16] S. Ong, W. Lee, P. Keng, S.T. Ha, Equilibrium studies and kinetics mechanism for the removal of basic and reactive dyes in both single and binary systems using EDTA modified rice husk, International, J. Phys. Sci. 5 (2010) 582–595.
[17] C.S. Babu, C. Chakrapani, K.S. Rao, Equilibrium and kinetic studies of reactive Red2 Dye adsorption onto prepared activated-carbons, J. Chem. Pharm. Res. 3 (2011) 428–439.
[18] P. Pengthamkeerati, T. Satapanajaru, O. Singchan, Sorption of reactive dye from aqueous solution on biomass fly ash, J. Hazard. Mater. 153 (2008) 1149–1156.
[19] Y.S. Al-Degs, I.M. El-Barghouth, A.H. El-Sheikh, G.M. Walker, Effect of solution pH, ionic strength, and temperature on adsorption behavior of reactive dyes on activated carbon, Dyes Pigm. 77 (2008) 16–23.
[20] S.J. Allen1, B. Koumanova, decolourisation of water/wastewater using adsorption, J. Univ. Chem.Technol. Metall. 40 (2005) 175–192.
[21] N.K. Lazaridis, T.D. Karapantsios, D. Georgantas, Kinetic analysis for the removal of a reactive dye from aqueous solution onto hydrotalcite by adsorption, Water Res. 37 (2003) 3023–3033.
[22] F. Wo, R. Tseng, R.S. Juang, Kinetic modeling of liquid phase adsorption of reactive dyes and metal ions on chitson, Water Res. 35 (2001) 613–618.
[23] N.K. Yahaya, M.F. Latiff, O.S. Bello, M. Ahmed, Fixed-bed column study for Cu (II) removal from aqueous solutions using rice husk based activated carbon, Int. J. Eng. Technol. 11 (2011) 248–252.
[24] L. Markovska, V. Meshko, V. Noveski, Adsorption of Basic Dyes in a Fixed Bed Column Korean J, Chem. Eng. 18 (2001) 190–195.